Performance and Thermal Characterization of the NASA-300MS 20 kW Hall Effect Thruster

IEPC-2013-444

Presented at the 33rd International Electric Propulsion Conference,
The George Washington University • Washington, D.C. • USA
October 6 – 10, 2013

Hani Kamhawi[*], Wensheng Huang.[†], Thomas Haag[‡], Rohit Shastry[§], George Soulas[**], Timothy Smith[††]
National Aeronautics and Space Administration Glenn Research Center, Cleveland, Ohio, 44135

and

Ioannis Mikellides[‡‡], and Richard Hofer[§§]
Jet Propulsion Laboratory, Pasadena, California

NASA's Space Technology Mission Directorate is sponsoring the development of a high fidelity 15 kW-class long-life high performance Hall thruster for candidate NASA technology demonstration missions. An essential element of the development process is demonstration that incorporation of magnetic shielding on a 20 kW-class Hall thruster will yield significant improvements in the throughput capability of the thruster without any significant reduction in thruster performance. As such, NASA Glenn Research Center and the Jet Propulsion Laboratory collaborated on modifying the NASA-300M 20 kW Hall thruster to improve its propellant throughput capability. JPL and NASA Glenn researchers performed plasma numerical simulations with JPL's Hall2De and a commercially available magnetic modeling code that indicated significant enhancement in the throughput capability of the NASA-300M can be attained by modifying the thruster's magnetic circuit. This led to modifying the NASA-300M magnetic topology to a magnetically shielded topology. This paper presents performance evaluation results of the two NASA-300M magnetically shielded thruster configurations, designated 300MS and 300MS-2. The 300MS and 300MS-2 were operated at power levels between 2.5 and 20 kW at discharge voltages between 200 and 700 V. Discharge channel deposition from back-sputtered facility wall flux, and plasma potential and electron temperature measurements made on the inner and outer discharge channel surfaces confirmed that magnetic shielding was achieved. Peak total thrust efficiency of 64% and total specific impulse of 3,050 sec were demonstrated with the 300MS-2 at 20 kW. Thermal characterization results indicate that the boron nitride discharge chamber walls temperatures are approximately 100 °C lower for the 300MS when compared to the NASA-300M at the same thruster operating discharge power.

I. Introduction

High power electric propulsion systems are enabling and enhancing missions requiring transportation of large payloads. A number of mission studies were performed highlighting the enhancing and enabling features of

[*] Senior Research Engineer, Propulsion and Propellants Branch, hani.kamhawi-1@nasa.gov.
[†] Research Engineer, Propulsion and Propellants Branch,wensheng.huang@nasa.gov.
[‡] Senior Propulsion Engineer, Space Propulsion Branch, thomas.w.haag@nasa.gov.
[§] Senior Research Engineer, Propulsion and Propellants Branch,george.c.soulas@nasa.gov.
[**] Research Engineer, Propulsion and Propellants Branch,rohit.shastry@nasa.gov.
[††] Project Manager, Space Technology Project Office, timothy.d.smith@nasa.gov
[‡‡] Senior Research Scientist, Electric Propulsion Group, ioannis.g.mikellides@jpl.nasa.gov.
[§§] Senior Research Engineer, Electric Propulsion Group, richard.d.hofer@jpl.nasa.gov.

high power EP systems for reusable space tug applications for transfer of payloads from LEO to GEO and for use in Mars mission scenarios.[1,2,3]

NASA Glenn Research Center, thereafter referred to as NASA Glenn, has a long history of researching and developing high power Hall thrusters. Testing of high power Hall thruster was performed at NASA Glenn as early as 1998.[4] Since that time NASA Glenn has designed, fabricated, and tested a number of high power Hall thrusters including the NASA-457M-v1 &v2, NASA-400M, and NASA-300M. [5,6,7,8,9] However, in 2004 funding for the development of high power EP thrusters was drastically reduced and a number of high power thruster development activities were eliminated including projects at NASA Glenn that were developing and testing 20 and 50 kW Hall thrusters.

National interest in high-power EP systems has been renewed. In 2010, NASA's Human Exploration Framework Team (HEFT) concluded that the use of a high-power (i.e., on the order of 300 kW) solar electric propulsion (SEP) system could significantly reduce the number of heavy lift launch vehicles required for a human mission to a near Earth asteroid.[10] Hall thrusters are ideal for such applications because of their high-power processing capabilities and their efficient operation at moderate specific impulses (~2000 sec), which leads to reduced trip times for such missions.[11]

NASA's Human Exploration and Operations Mission Directorate (HEOMD) Enabling Technology Development and Demonstration (ETDD) Program was focused on developing, maturing, testing, and demonstrating the technologies needed to reduce the cost and expand the capability of future space exploration activities. The ETDD Program content included performing foundational research and studying of the requirements and potential designs of advanced, high-energy in-space propulsion systems. These high-energy propulsion systems were intended to support deep space human exploration and reduce travel time between Earth's orbit and future destinations for human activity. This would enable a new space transportation capability via a solar electric propulsion (SEP) stage. The SEP stage could enable cost-effective missions within Earth orbit, near Earth objects (NEOs), and deep space robotic science missions. In 2011, the ETDD Program transitioned to NASA's Office of the Chief Technologist (OCT) but the program content remained mostly unchanged. To that extent, there are several projects in the OCT Game Changing Division (GCD) that support technology development which will result in the SEP Technical Demonstration Mission (TDM) flight development. One of the key projects under OCT GCD is the In-Space Propulsion (ISP) project which is pursuing the development of high-power, long-life Hall thruster in support of SEP TDM.[12] In 2012, NASA's OCT office was transitioned into the newly formed Space Technology Mission Directorate (STMD). Under STMD the content of the ISP project was unchanged.

In 2011 and 2012, the focus of the OCT/STMD ISP project activities at NASA Glenn, was evaluating the performance of the NASA-300M (20 kW) and NASA-457Mv2 (50 kW) thrusters,[13,14] and the development of internal, near and far-field plasma diagnostics.[15,16,17]

Most recently, the asteroid redirect mission (ARM) has been included as one of the candidate SEP TDMs. High-power SEP would be enabling for the exploitation of asteroid resources. The design of a 40-kW end-of-life SEP system was presented by Brophy *et al*.[18] The high power SEP system would enable the spacecraft to rendezvous with, capture, and subsequently transport a 1,000-metric-ton near-Earth asteroid back to cislunar space. The asteroid redirect mission benefits from a Hall thruster capable of operating at specific impulse up to 3,000 sec.

One of the major ISP tasks is the development and demonstration of a high-fidelity, long-life, high-performance 15 kW-class Hall thruster that incorporates technologies that are extensible to a 300 kW Hall propulsion system. To that end, the recent tests of the NASA-300M and NASA-457Mv2 thruster have demonstrated NASA's capability to design, fabricate, and test high power high performance Hall thrusters. Recent tests at JPL with the H6 (6 kW) thruster have shown that magnetic shielding has the potential to improve Hall thruster life by ten orders of magnitude.[19]

The main objective of the work presented in this paper is demonstration that magnetic shielding can be implemented on 20 kW-class Hall thruster and will result in significant improvements in the throughput capability of high power Hall thrusters. To achieve this main objective, NASA Glenn and JPL researchers teamed together to implement magnetic shielding on the NASA-300M.

This report is organized in 5 sections. Section II presents the design methodology employed in modifying the NASA-300M thruster to attain magnetic shielding. Section II also provides a brief description of magnetic shielding and JPL's Hall2De code, the Hall2De simulation results of the NASA-300M, and NASA-300M magnetically shielded thruster are discussed. Section III presents the experimental apparatus (test hardware, facilities, supporting systems, and plasma diagnostics) used in this test campaign. Section IV presents and discusses the experimental results which include photographs of the thruster discharge chamber, summary of discharge channel surface plasma measurements, and thruster performance results. Section V presents a brief discussion of the thermal characterization tests that were performed during this test campaign. Section VI presents conclusions.

II. Thruster Design Methodology

The methodology employed to modify the original design of the NASA-300M Hall thruster also referred thereafter as the "unshielded" or "US" configuration, followed closely that used in a recent effort at the Jet Propulsion Laboratory that led to the demonstration of magnetic shielding in a 6-kW laboratory Hall thruster called the H6MS.[20,21,22] The physics-based 2-D axisymmetric plasma code Hall2De[23] has been used to guide modifications to the magnetic circuit of the NASA-300M. The plasma simulations were combined with modeling of the magnetic circuit using MagNet (v7), a 2-D/3-D electromagnetic field simulation software developed by Infolytica Corporation[24] that has been used for many years at various institutions of government, industry and academia to design magnetic circuits for Hall thrusters. The modeling effort produced a magnetically shielded (MS) configuration we will denote in this paper as the 300MS-0. Section IIc reports on numerical simulation results for both the US configuration, the 300M, and the first MS configuration, the 300MS-0. Based on the simulation results, a few iterations on the MS configuration ensued that produced minor changes in the magnetic field topology of the 300MS-0 design. The channel chamfering geometry was also slightly changed but to an extent that did not exceed ~1mm. Two configurations were ultimately tested that will be referred to herein as well as in our companion papers by Rohit *et al*. [25] and Wensheng *et al*. [26] as the 300MS and 300MS-2.

A. Magnetic Shielding in Hall Thrusters

The first principles of magnetic shielding have been described in detail in previous articles by Mikellides *et al*.[27,28] Therefore in this section we provide only a brief description for completeness. Under the discharge conditions established in Hall thrusters, the resistance to the transport of heat and mass in the electron flow in a direction parallel (||) to the applied magnetic field **B** is much smaller (by $\sim\Omega_e^2$ where Ω_e is the electron Hall parameter) than that in the $\perp$ direction for most of the channel region. Thus, the electron temperature T_e remains relatively unchanged along the lines of force:

$$\nabla_{\parallel} T_e \approx 0 . \tag{1}$$

Moreover, in the absence of a resistive contribution to the electric field **E** in this direction the electron momentum equation simplifies to:

$$\mathbf{E}_{\parallel} \approx -T_e \nabla_{\parallel} \ell n(n_e), \tag{2}$$

where n_e is the electron number density. Equations (1) and (2) yield respectively two well-known properties of the lines of force in these thrusters[29,30]: $T_e \approx T_{e0}$ and $\phi \approx \phi_0 + T_{e0}\ell n(n_e/n_{e0})$ along a magnetic field line, where T_{e0}, ϕ_0 and n_{e0} denote integration constants and ϕ is the plasma potential. Thus, though each line is nearly isothermal, it is not also of fixed potential unless the electron temperature is zero.[30] This allows for a finite component of **E** parallel to **B** which, in turn, can lead to ion acceleration towards the containing walls if the **B-**lines begin/terminate at the surface of the material. Erosion of the channel walls occurs when ions strike them with sufficient energy to sputter off material.

Deviations from equipotentiality along lines of force near the channel walls has been the main reason that most state-of-the-art Hall thruster designs have continued to exhibit channel erosion. To better illustrate the main impediment we use as an example of a typical SPT-like magnetic field configuration as depicted in Fig.1-middle. We designate this as the "US configuration." Here the variation of ϕ and T_e along the walls is similar to that along the CL because the lines are nearly radial. Consequently, the elevated $E_{||}$ and T_e at the walls can drive a flux of high-energy ions to the walls. Referring to Fig.1-right, magnetic shielding is achieved by way of a magnetic field topology that sustains high ϕ and low T_e near the channel surfaces, in fact, as close as possible to the discharge voltage V_d and to the coldest values of T_e that can be attained inside the channel, respectively. In this manner the incident-ion kinetic and sheath energies can be marginalized. Moreover, with a properly designed combination of **B** and channel geometry, **E** can be controlled to be both nearly perpendicular to the surface and large in magnitude, as shown in the MS configuration Fig.1-right. That is, magnetic shielding seeks to achieve ideal equipotentialization of the lines of force near the walls. In this manner the induced $\mathbf{E}_{\perp}$ forces ion acceleration away from walls without loss of thruster performance. This also reduces the wall-incident ion flux. A change in the geometry of the wall alone, e.g. chamfering of the surface, is not sufficient as it has been demonstrated in recent tests.[21] The key principle behind magnetic shielding lies in the recognition that the electron pressure (yielding $T_e \times \ln(n_e)$ in Eq. (2)) forces **E**

and **B** to no longer form an orthogonal set (Fig.1-middle)**.** Thus, a geometry of **B**-lines with convex curvature toward the anode[31] cannot effectively control **E** near surfaces (and, in turn, the erosion) if the near-wall lines are not also equipotential. In contrast, Fig.1-right shows a magnetically shielding **B** topology. This topology eliminates the contribution of the electron pressure by exploiting those **B**-lines that extend deep inside the acceleration channel, near the anode. Because these lines are associated with high ϕ_0 and low T_{e0} the contribution of $T_e \times \ln(n_e)$ is marginalized.

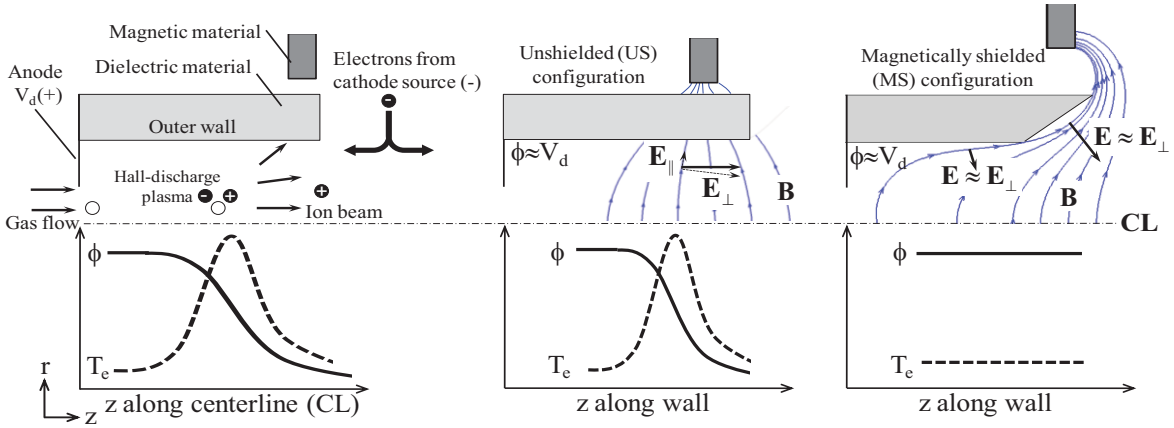

Figure 1. Schematics of the upper half of the annular acceleration channel in a typical magnetic-layer Hall thruster (top) and typical profiles of ϕ and T_e (bottom) established during ion acceleration (from Mikellides, *et al.*[28]). Left: Basic features of the accelerator and typical profiles along the CL. Middle: Representative magnetic field lines and profiles along the wall in a US configuration. Right: Representative magnetic field lines and profiles along the wall in a MS configuration. The line that extends deepest into acceleration channel and runs closest to the channel wall without crossing shall be called the "grazing line."

B. General description of the Hall2De code

The numerical simulations have been performed with the Hall2De code,[23,32] a two-dimensional (2-D) computational solver of the conservation equations that govern the evolution of the partially ionized gas in Hall thrusters. The governing equations, numerical methodology, various thruster simulations and comparisons with measurements have been presented elsewhere.[20,22,23] Here, we provide only a brief overview of the code for completeness.

Excessive numerical diffusion due to the large disparity of the transport coefficients parallel and perpendicular to the magnetic field is evaded in Hall2De by discretizing the equations on a computational mesh that is aligned with the applied magnetic field. The magnetic-field-aligned-mesh (MFAM) capability in Hall2De was largely motivated by the need to assess the life of Hall thrusters with complicated magnetic field topologies. Shown in Fig.2 is a schematic of the computational domain used in the 300M simulations with naming conventions of various thruster components and boundaries. The MFAM spans a computational domain in r-z geometry that extends several times the thruster channel length in the axial direction, and encompasses the cathode boundary and the thruster CL. The numerical solution of the conservation equations for the heavy species is obtained without invoking discrete-particle methods. The evolution of the (collisionless) neutral species is computed using line-of-sight formulations that account for ionization.[32] Ions are treated as an isothermal, cold (relative to the electrons) fluid, accounting for the drag force and the ion-pressure gradient. Up to triply-charged ions and up to four distinct ion fluids can be included in Hall2De. In the 300M and 300MS-0 simulations presented here, three charge states were accounted for, but all ions were considered to be part of a single fluid. The electron population in Hall2De is treated also as a fluid. The solution of the electron energy conservation equation provides T_e. Ohm's law is solved in the frame of reference of the magnetic field with the electrical resistivity accounting for contributions from collisions of electrons with all other species. It is argued that the diffusion of electrons in Hall thrusters is enhanced in a non-classical manner by plasma turbulence.[33,34] In numerical simulations this enhancement has typically been modeled using an effective or "non-classical" collision frequency. Denoting this collision frequency as ν_α, we impose in Hall2De a so-called transport coefficient function $f_\alpha(r,z)$ and set

$$\nu_\alpha = f_\alpha \omega_{ce} . \tag{3}$$

Our specification of f_α is guided by plasma measurements whenever they exist. In the present simulations plasma only electron temperature measurements were used that spanned both the interior of the acceleration channel and the plume region. At the time these simulations were performed, no additional measurements were available.

The conservation equations for the electrons are closed with boundary conditions (BC) at all surfaces shown in Fig.2. The channel (ring) walls and the thruster front plate are dielectric boundaries. At the anode we impose sheath BCs for the electron current density normal to the anode. At the cathode boundary, the neutral particle flux, ion flux, plasma potential and electron temperature are specified. For all dielectric-wall boundaries a zero-current condition is imposed. At these surfaces the BC for the convective heat loss follows the formulations of Hobbs and Wesson[35] for the potential drop in a sheath with secondary electron emission. The far plume solution is subject to outflow BCs. The energy equation is solved in a semi-implicit fashion; the thermal conduction term is implicit whereas all other terms are evaluated explicitly. Current conservation, incorporating Ohm's law to solve for the electron current density, is also solved implicitly.

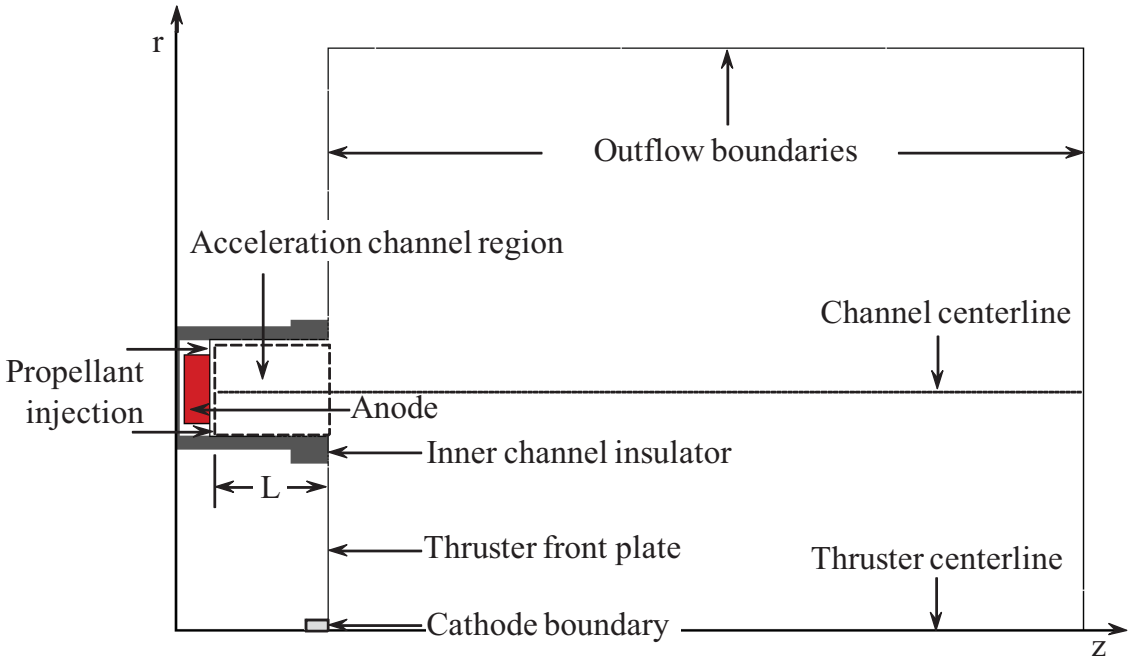

Figure 2. Computational domain for the numerical simulations of the NASA 300M and 300MS-0 showing naming conventions for various thruster components and boundaries to be cited throughout this paper.

C. Simulation results

In this section we present numerical simulations of the 300M and 300MS-0 operating with xenon at discharge voltage (V_d) of 500 V and discharge current (I_d) of 40 A. The remainder of the operating conditions required for the simulations such as anode and cathode flow rates were specified based on measurements. The channel geometry of this thruster is relatively simple and the hollow cathode is located at the thruster centerline as shown in Fig.2. This cathode-thruster arrangement is of great interest in numerical simulations because it is 2-D axisymmetric and therefore plasma measurements may be compared directly and unambiguously with the simulation results. The maximum axial and radial dimensions of the computational domain are $(z/L)_{max}$=7.4 and $(r/L)_{max}$=4.9, respectively where L denotes the length of the acceleration channel region (see Fig.2).

Plasma simulations for the 300M were performed first since internal measurements already existed in this configuration. The simulation results for ϕ and T_e along the axis of symmetry are plotted in Fig.3-left. Comparisons of the 300M results with T_e measurements in this configuration and with simulation results for the 300MS-0 are also shown in Fig.3-left. As also seen in the simulations of the H6MS thruster (e.g. see Ref 22), we find higher maximum T_e in the 300MS-0, by about 15 eV, compared to that in the 300M. Though such trends have not yet been seen consistently through the probe measurements, we have argued that this T_e enhancement in the MS configurations is largely due to the reduced electron energy losses to the walls and the inherently coalesced topology of the magnetic field away for the channel CL. We also find, as expected, that the location of the maximum T_e and axial electric field in the MS configuration is displaced downstream of that in the 300M configuration by approximately the same

distance as the maximum radial magnetic field. This is illustrated clearly in Fig.3-left. A comparison of the normalized radial magnetic field along the channel CL of the two configurations is plotted in Fig.3-right.

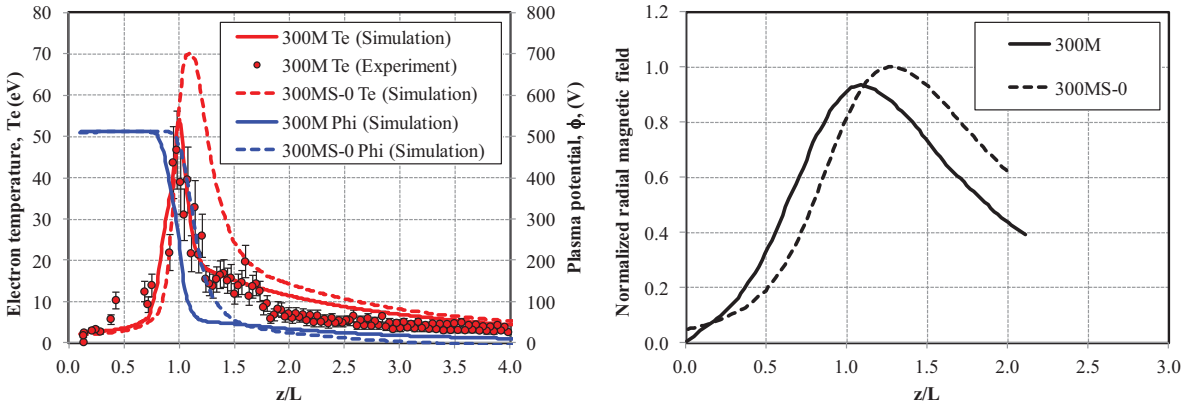

Figure 3. Axial profiles along the channel centerline from numerical simulations of the NASA 300M and 300MS-0. Left: Computed electron temperature and plasma potential. Also plotted are measurements of the electron temperature obtained by a fast-moving probe system at NASA GRC. Right: Normalized radial component of the applied magnetic field along the channel CL obtained by the MagNet solver.

The 2-D simulation results in the vicinity of the acceleration channel are compared in the 300M (left) and 300MS-0 (right) configurations in Fig.4. The effect of magnetic shielding on the plasma potential is evident in Fig.4-top. We compute a reduction in the plasma potential along the 300MS-0 diverging walls that does not exceed ~4 V, compared to a drop of almost 300 V along the 300M walls near the channel exit. The kinetic energy with which ions bombard the walls is therefore lowered significantly in the MS configuration. The plasma potential profiles along the walls are also plotted in Fig.5-left.

The same principle that leads to the thermalized equipotentialization of the lines of force is responsible also for their isothermalization. Thus, since magnetic field lines are nearly isothermal in the acceleration channel, those lines that graze the corner formed by the cylindrical and diverging sections of the channel wall in the 300MS-0 configuration are associated also with low values of the electron temperature because they extend deep into the acceleration channel. There the electrons are considerably colder as shown for example in Fig.3-left and Fig.4-center. The comparison of the two configurations (Fig.4-center-left and Fig.4-center-right) shows a significant reduction of the temperature in these highly shielded regions. Because the electron temperature is reduced, a decline of the sheath fall along these surfaces is also induced. The reduction of the electron temperature along the 300MS-0 walls compared to that in the 300M is also illustrated in Fig.5-right.

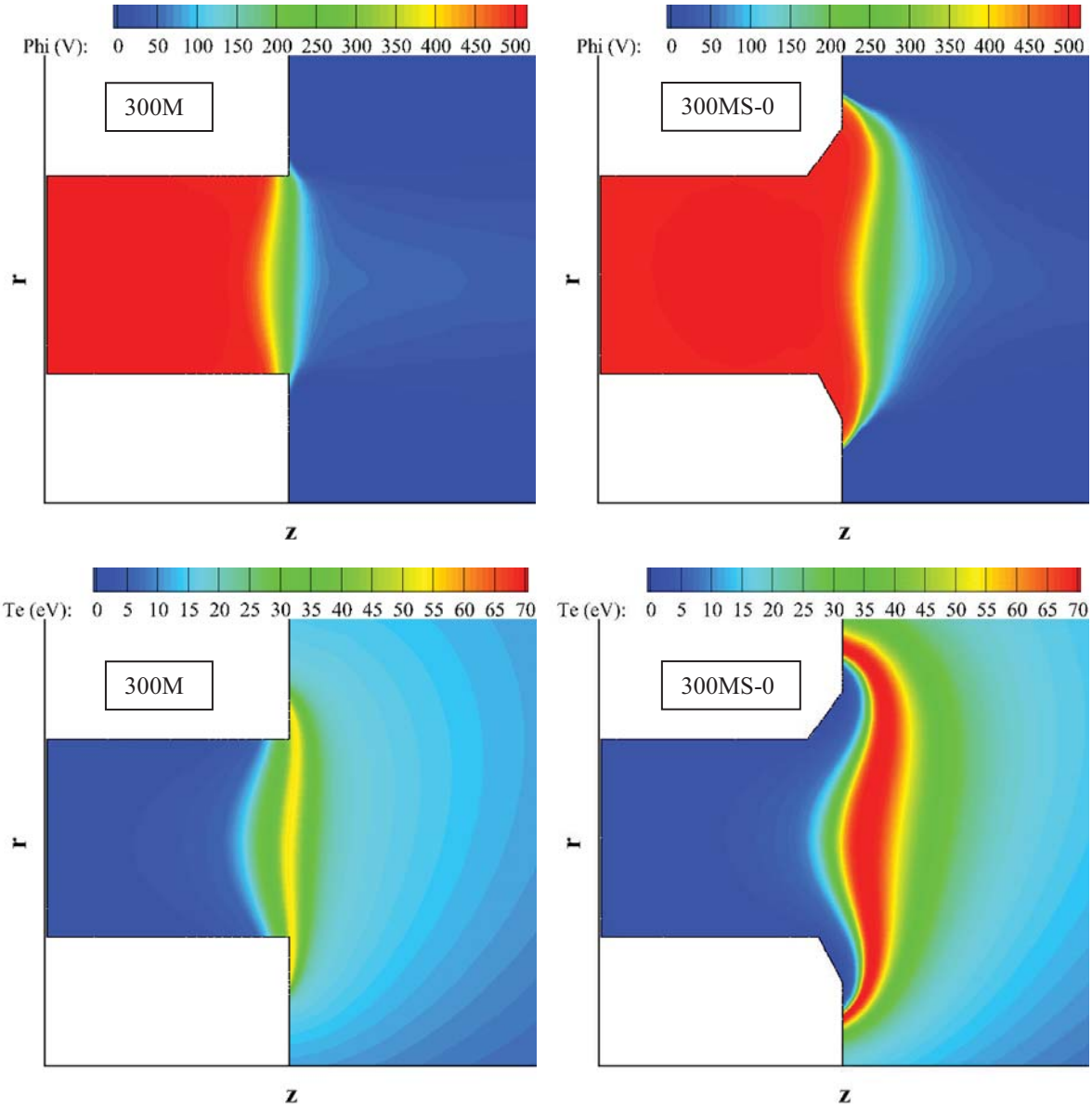

Figure 4. 2-D contours of the computed plasma potential (top) and electron temperature (bottom) in the NASA 300M (left) and 300MS-0 (right) configurations from numerical simulations with the Hall2De code.

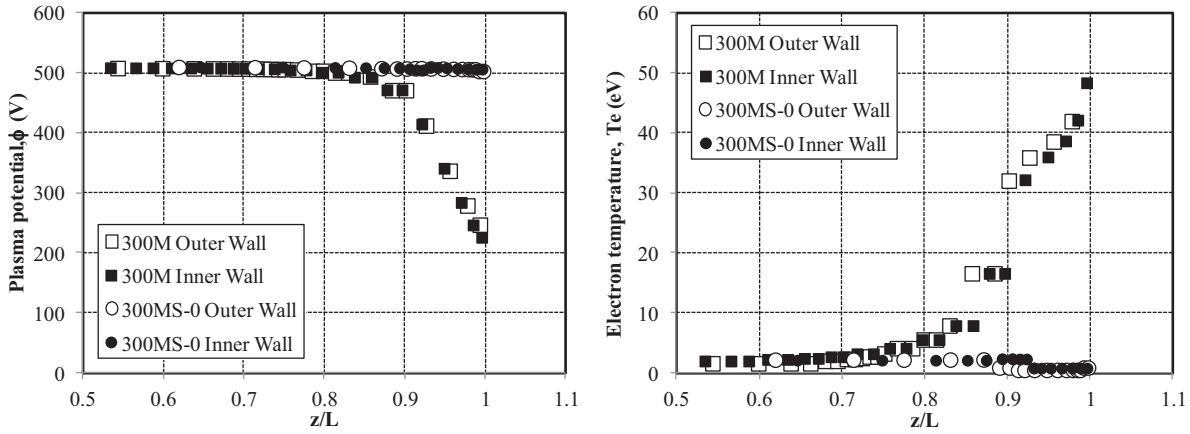

Figure 5. Hall2De results for the plasma potential (left) and electron temperature (right) along the walls of the NASA 300M and 300MS-0 configurations.

The plasma results were then used to quantify the erosion reductions along the channel walls. The computed erosion rates are compared for the two configurations in Fig.6. The approach for determining the erosion rates has been described in numerous other articles (for example, see Refs. 20, 22, 27). Briefly, the rates use the computed ion flux to the walls and a sputtering yield function that consists of fits for the angular and energy dependencies. In the results presented here we have used the fits reported in Refs. 20 and 22. We found that the erosion rate of the 300 MS-0 inner wall is reduced by more than three orders of magnitude. At the outer wall, we found that the ion energy was less than the sputtering yield threshold used (25 V) so no erosion was computed along this wall.

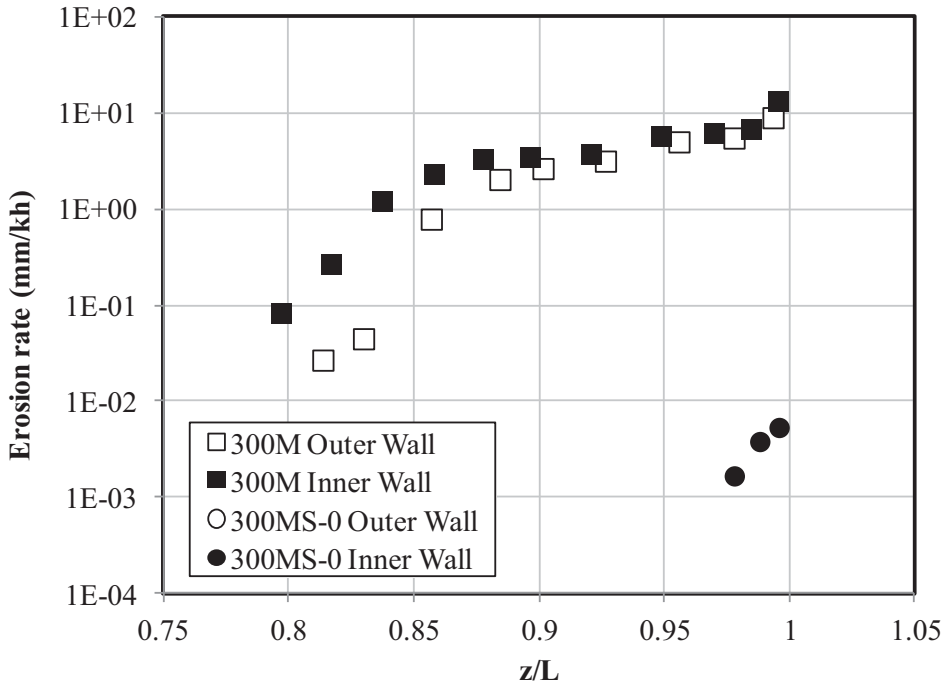

Figure 6. Computed erosion rates along the outer and inner channel walls of the NASA 300M and 300MS-0 configurations.

III. EXPERIMENTAL APPARATUS

The experimental apparatus used in evaluating the performance of the magnetically shield 300M thruster will be detailed in this section. The experimental hardware and facilities include the thruster (two configurations), hollow cathode assembly unit, vacuum facility 5 (VF5), a laboratory propellant feed system, power console, an inverted pendulum thruster stand, data acquisition system, and internal and far-field plasma probes.

A. The NASA-300MS Thruster and Hollow Cathode Assembly

The NASA-300M, thereafter referred to as the 300M, was designed in 2004 and its fabrication and assembly were completed in 2005. The 300M thruster was designed and fabricated under the support of the Exploration System Research and Technology (ESR&T) Program. The 300M design is based on a scaled version of the NASA-457Mv2. The 300M design incorporated lessons learned from the development and testing of the NASA-457Mv1, NASA-400M, and NASA-457Mv2 thrusters.[8] The goal of the design was to minimize the size of the design while optimizing the magnetic field and plasma lens to attain improved performance. The 300M nominal design specifications were: discharge power of 20 kW, discharge voltage range up to 600 V, discharge current up to 50 A, and a magnetic circuit that has a magnetic field topology similar to the NASA-457Mv2. The thruster's anode was manufactured by the Busek Company. For this study the magnetic circuit of the 300M was modified to be able to achieve a magnetically shielded field topology. A number of several design approaches could have been pursued for modifying the magnetic topology of the 300M to a magnetically shielded topology, however, the design team at NASA Glenn decided that it was important to preserve the baseline 300M magnetic topology and be able to revert to that at any time. This restricted and limited our ability to attain the exact magnetic field topology that was modeled in Hall2De (300MS-0). To preserve the original 300M magnetic configuration, new magnetic circuit components were added to the existing 300M magnetic circuit components in order to attain a magnetically shielded field topology. No modifications (except for drilling a number of small sized holes) were performed on the 300M magnetic circuit elements. The design of the additional magnetic circuit components was guided by detailed magnetic field simulations performed with MagNet v7.[24] A new boron nitride discharge chamber with a chamfered exit plane on both the inner and outer boron nitride walls was fabricated for the 300MS. For the test campaign that is reported in this study, two 300MS thruster configurations were tested. Configuration 1, designated 300MS, incorporated the magnetically shielded field topology and preserved the discharge channel aspect ratio of the original 300M. Configuration 2, designated 300MS-2, had the same magnetic field topology as the 300MS with the only difference being that the discharge chamber was shortened by 20%, that was achieved by advancing the anode forward from its baseline position. This was done to investigate the effect of shortening the discharge chamber on the performance of a magnetically shielded Hall thruster. Figure 8 shows a photograph of the 300MS mounted on the inverted pendulum thrust inside NASA Glenn's vacuum facility 5 (VF5).

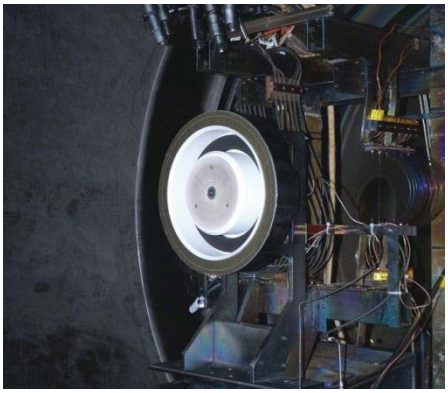

Figure 8. Photograph of the 300MS thruster inside VF5 prior to testing.

Figure 9. Photograph of high current hollow cathode unit used in testing.

The laboratory hollow cathode assembly unit used in this test campaign is the same unit used in testing of the NASA-457Mv1and v2, 300M, and NASA-400M thrusters. The hollow cathode assembly unit is based on the discharge cathode assembly unit for NASA's Evolutionary Xenon Thruster (NEXT) thruster with modification to the cathode and keeper orifice diameters. Figure 9 shows a photograph of the hollow cathode assembly unit. For this test campaign, the cathode flow rate was maintained at 8% of the anode flow rate.

B. Vacuum Facility 5

Testing of the 300MS and 300Ms-2 was performed in VF5 at NASA Glenn. VF5 main chamber is 4.6 m in diameter and is 18.3 m long, VF5's main port (designated E55) is 1.8 m in diameter and is 2.5 m long. Vacuum facility 5 can be evacuated with cryopanels and oil diffusion pumps. For the 300M test only the cryopanels were used to evacuate the facility. Facility pressures were monitored with six ion gauges. One of the ion gauges was a

Stabil ion gauge and it was mounted next to the thrust stand. Facility pressure uncertainties were estimated by the manufacturer to be within ±6% of reading. The pressure reading made with the Stabil ion gauge, corrected for xenon, next to the thrust stand was less than 3.5×10^{-3} Pa (2.6×10^{-5} Torr) throughout testing.

C. Laboratory Feed System

A laboratory propellant feed system was used in testing of the 300M thruster. The propellant feed system utilized two mass flow controllers (MFCs). For the anode flow, a 1 SLM MFC was used, while for the hollow cathode flow, a 200 SCCM MFC was used. Both MFCs were calibrated prior and after testing. The MFC calibration curves indicated that the anode and cathode flow rates uncertainty is ≤1% of set value.

D. Power Console

The discharge power supply used during 300M test campaign is a 200 kW supply that is capable of supplying 2000 V at 100 A and had a built in 5.5 mF output filter capacitance. A 15.3 mF capacitor bank was connected in parallel with the power supply at the thruster's vacuum facility electrical feed-throughs to filter discharge current oscillations. The cathode heater, cathode keeper, and electromagnet power supplies were laboratory units that are capable of supplying up to 18A. The output of the power supplies was calibrated (in conjunction with data acquisition system) prior to testing. Calibration curves indicated that discharge power can be measured to within 1%.

E. Inverted Pendulum Thrust Stand

A Null-type water-cooled inverted pendulum thrust stand was implemented during thruster performance evaluation. The power cables were fed from the vacuum feed-throughs to the thruster using a "water fall" configuration to minimize the thermal drift of the thrust stand readings. In-situ thrust stand calibrations were performed prior, during, and after thruster testing. In addition, during thruster testing the thruster was periodically turned off to measure the thrust stand thermal drift magnitude, and the corrections were incorporated in the reported thrust. Thrust measurement uncertainty was estimated at 2% of measured value. During testing, the thrust stand temperature was maintained at 23 °C, and thrust stand maximum thermal drift was approximately 10 mN.

F. Data Acquisition

A data logger was used to measure and record the thruster operating parameters. The data logger measurements were calibrated using a calibrated meter. The uncertainty in the data logger readings were incorporated in the uncertainties reported earlier for the power and thrust stand measurements.

G. Plasma Diagnostics

A number of internal, and far-field plasma diagnostics were implemented during this test campaign and they include:

- Surface flush-mounted Langmuir probes as well as a cylindrical Langmuir probe. The flush-mounted Langmuir probes were used to determine the electron temperature and plasma potential on the chamfered portion of the inner and outer channel surfaces near the thruster exit plane. The cylindrical probe was primarily used to measure the spatial variations in electron temperature within and just downstream of the thruster channel on the 300MS configuration. The probe was mounted on a high-speed axial reciprocated probe (HARP) system. The cylindrical probe plasma measurements will be used to help validate the Hall2De simulation results. Figure 10 shows the general setup used for the flush mounted Langmuir probes and internal cylindrical Langmuir probe measurements. Detailed description of the setup and data acquisition approach is presented in a companion paper by Rohit *et. al*.[25]
- Far-field Langmuir probe, retarding potential analyzer (RPA), and an ExB probe were mounted on a probe tower with accompanying shielding and shutters protecting the RPA and the ExB probe. This far-field probe tower was attached to a vertical motion stage located ~27 mean thruster diameter (MCD) downstream of the thruster exit plane and sitting behind a body shield. During the data acquisition process, each probe was moved vertically to a point roughly along the central axis of the thruster before measurements were taken. The probe tower retreated behind the shield once data acquisition was completed. A NASA Glenn designed far-field Faraday probe was used to measure ion current density. It was mounted onto a commercially available three-axis belt-driven motion system. The motion system provides 2D rectilinear motion and probe rotation. The Faraday probe was set at 5 MCD away from the thruster because it needed to be far enough away from the

thruster for the source of the thruster exhaust to be considered a point source. Figure 11 shows a photograph of the diagnostics setup inside VF5 and a close up of the far-field probe tower. Analysis of the test data is presented in a companion paper by Huang *et al*.[26]

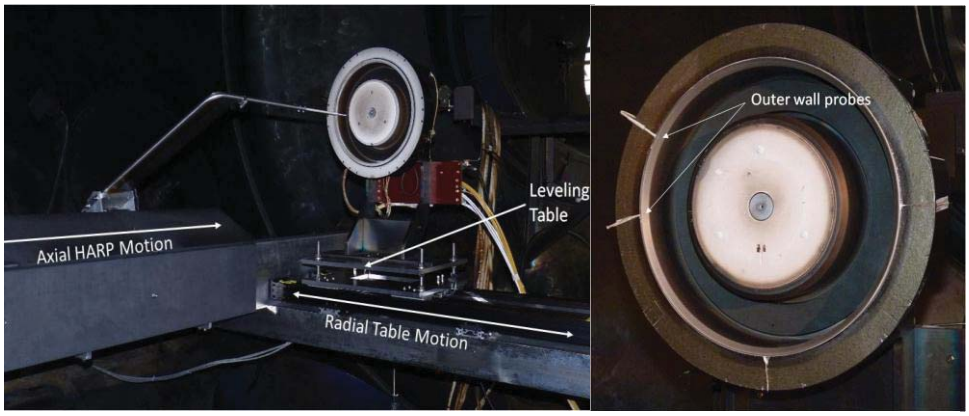

Figure 10. Photographs of the thruster and probe setup for the cylindrical and surface flush-mounted Langmuir probes during Test#3 at NASA Glenn VF5.

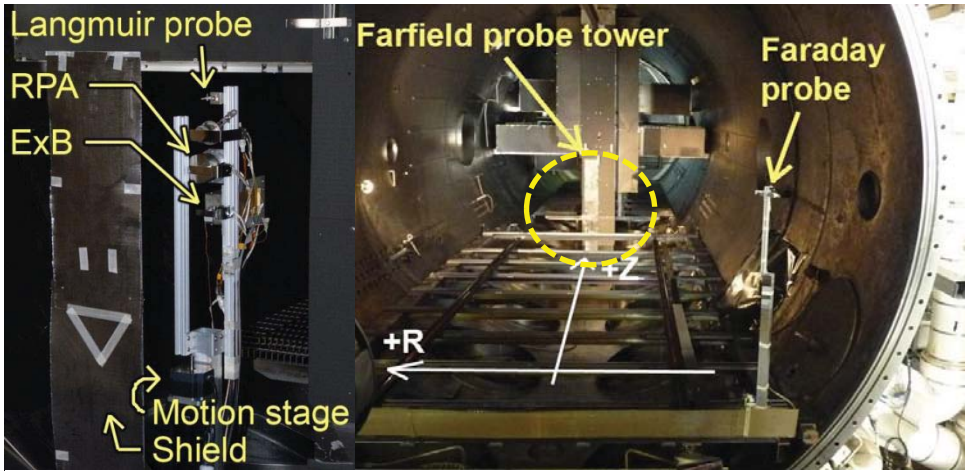

Figure 11. Photographs of the far-field plasma probes layout inside VF5 for Test#1 and #2.

The current test campaign included execution of three test entries and they were:

1. Test #1 included evaluating the performance of the 300MS at power levels between 2.5 and 20 kW for discharge voltages between 200 and 600 V;
2. Test#2 included evaluating the performance of the 300MS-2; this was performed at power levels between 2.5 and 20 kW for discharge voltages between 200 and 700 V; and
3. Test#3 incorporated performing plasma measurements along the discharge chamber inner and outer surfaces with flush-mounted Langmuir probes on the 300MS. In addition, Langmuir probe axial sweeps were performed within the discharge chamber at different radial locations as is reported in a companion paper.[25] Finally, during Test#3, key 300MS thruster components including the discharge channel walls (inner and outer), outer front pole, inner electromagnet, and backpole were instrumented with type-K thermocouples to characterize the thermal operation of the thruster and to compare with test results from the 300M.

For test entries 1 and 2 far-field Faraday probe, EXB, and RPA measurements were performed and the results are presented in a companion paper by Huang *et al*.[26]

IV. Experimental Results and Discussion

This section discusses the experimental results that were obtained during the 300MS and 300MS-2 tests. Those results include visual verification of magnetic shielding attainment. A summary of the results from the surface flush mounted Langmuir probe measurements will be presented to demonstrate why the NASA Glenn and JPL team members strongly feel that magnetically shielding was achieved in the 300MS thruster. Then the 300MS and 300MS-2 thrusters performance results will be presented and will be compared to the 300M (US) results. Finally, a summary of key findings from the thermal characterization test will be presented and discussed.

A. Magnetic Shielding Demonstration

In Hall thrusters, ion impingement on the discharge channel walls (typically boron nitride) results in a "smooth white" band denoting and marking where the ions struck the channel. This smoothing and slight chamfering (if enough operational hours are accumulated) is due to direct ion bombardment that results in the sputter erosion of the discharge channel walls and removal of any back sputtered material that deposits on the discharge channel surfaces. Figure 12 shows a photograph of the 300M discharge channel inner and outer surface after hundreds of hours of operation, the images in Fig. 12 clearly display the "white smooth" band that was caused by the sustained ion bombardment.

Figure 12. Photograph of the 300M discharge channel inner and outer surfaces showing the "white smooth" band that appears due to ion bombardment.

A magnetically shielded thruster design, as stated earlier, is characterized by high ϕ_0 (preferably at anode potential) and low T_e along the discharge channel inner and outer surfaces. In addition, the induced $\mathbf{E}_\perp$ forces ion acceleration away from walls which reduces the wall-incident ion flux, and dramatically reduces discharge channel surface erosion. As such, a preliminary assessment of whether magnetic shielding has been achieved is made by visual inspection of the thruster discharge channel surfaces after accumulating tens of hours of operation. If deposition of back sputtered materials from the facility is observed on the discharge channel surfaces (particularly surfaces close to the channel exit plane) then that is a positive indication that the discharge channel surfaces are exhibiting a reduced ion flux and hence achievement of some level of magnetic shielding.

Figure 13 shows photographs of the 300MS at the beginning of the test campaign, after 49 hours, and after completion of Test#3 (99 hours of accumulated test time). From Fig. 13 and after 49 hours, the inner and outer discharge walls are visibly much darker than at the beginning of the test. Figure 13 also shows that after 99 hours the discharge channel walls are even darker than at 49 hours due to the additional deposition of back sputtered materials. There are indications that ion bombardment on the inner front pole boron nitride cover plate is occurring. Future tests will quantify and characterize the plasma properties and ion energies that may be impacting that inner front pole area.

Figure 14 presents close-up photographs of the 300MS inner and outer discharge channel walls after 99 hours of testing at the 6 and 9 o'clock positions. The images presented in Fig. 14 shows that the discharge channel walls are covered with back-sputtered materials. There seems to be no sputtering of the discharge channels surfaces (inner or outer) and that there is no observable evidence of the formation of a "smooth white" band anywhere along the inner or outer channel surfaces. Witness plates were mounted on the outer front pole and at the base of the thruster, the witness plates are being analyzed to help quantify the back sputter rate and the materials types that are depositing on the witness plates.

Figure 13. Photographs of the 300MS thruster inside NASA Glenn's VF5 prior to test initiation (left), after 49 hours (middle), and after 99 hours (right).

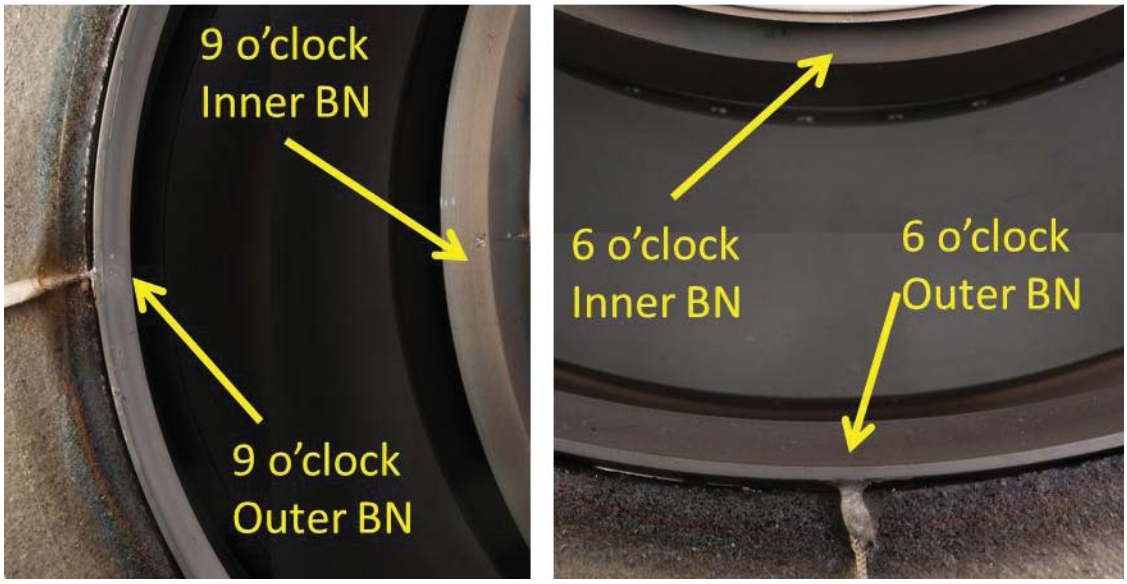

Figure 14. Photographs of the 300MS thruster discharge channel inner and outer walls after 99 hours of testing, 9 o'clock (left), 6 o'clock (right).

Definite confirmation that magnetic shielding was achieved in the 300MS was obtained when Test#3 was performed and its data analyzed. Detailed analysis of the surface flush-mounted Langmuir probes data is presented in a companion paper by Shastry *et al.*, but a summary of Shastry's findings will be included in this paper.[25] Results presented in Table 1 indicate that the plasma properties between the inner and outer surfaces are highly consistent, even when leakage current was observed on the inner wall probe. For all operating conditions, measured plasma potentials (always referenced to cathode potential) are slightly higher than anode potential. This indicates that ions near the discharge channel surfaces will have a negligible amount of beam ion energy. For most operating conditions, the measured electron temperatures were around 5 eV. This indicates a small of amount of sheath ion energy at the wall as well. However, at 400 V, 20 kW and 600 V, 20 kW, elevated temperatures around 10 eV were observed. The reason behind these elevated temperatures is still under investigation.[25]

Table 1. Measured plasma potentials and electron temperatures at the inner and outer walls of the 300MS, near the thruster exit plane. All plasma potentials are with respect to cathode potential. Magnetic shielding was achieved at all operating conditions. Values with an asterisk were calculated from data that exhibited signs of leakage current.

	Inner Wall		Outer Wall	
Operating Condition	*Plasma Potential [V]*	*Electron Temperature [eV]*	*Plasma Potential [V]*	*Electron Temperature [eV]*
300 V, 10 kW	310	4	305	5
300 V, 15 kW	311	6	304	4
400 V, 15 kW	410*	7*	402	5
400 V, 20 kW	413*	11*	408	11
500 V, 20 kW	508*	6*	501	5
600 V, 20 kW	600*	11*	603	12

B. Performance Characterization

One of main objectives of the undertaken test campaign is to evaluate the performance of a 20 kW-class magnetically shielded Hall thruster to assess whether magnetic shielding results in any thruster performance loss. To complete this assessment and to gain a better understanding of potential loss mechanism that may arise in this new magnetically shielded thruster configuration, the 300MS and 300MS-2 configurations performance were evaluated. An inverted pendulum thrust stand along with detailed far-field plume measurements were made to elucidate the thruster's performance and loss mechanisms. This section will detail and discuss the thruster performance at the various thruster operating points. A detailed presentation of the 300MS and 300MS-2 far-field plume measurements and analysis is presented in a companion paper by Huang *et al*.[26]

For this test campaign the performance of the 300MS and 300MS-2 configurations were evaluated at power levels between 2.5 and 20 kW. For the 300MS-2 configuration, tests were also performed at discharge voltage of 650 and 700 V to characterize performance at high discharge voltages. Table 2 below lists the various thruster operating conditions.

Table 2 lists thruster performance test matrix for configurations 300MS (gray) and 300MS-2 (yellow)

V_d, V	Thruster Discharge Power, kW															
	2.5		5		7.5		10.0		12.5		15.0		17.5		20.0	
300	•	•	•	•	•	•	•	•	•		•	•				•
400	•		•	•	•	•	•	•	•		•	•	•		•	•
500			•	•	•	•	•	•			•	•			•	•
600			•		•	•	•	•	•		•	•			•	•
650																•
700																•

The discharge specific impulse (I_{sp}) and thrust efficiency (η_t) of the thruster were calculated using

$$(I_{sp})_d = \frac{T}{\dot{m}_a g} \quad \text{and} \quad (\eta_t)_d = \frac{T^2}{2\dot{m}_a P_d} \qquad (4) \text{ and } (5)$$

Total specific impulse and efficiency were calculated using

$$I_{sp} = \frac{T}{(\dot{m}_a + \dot{m}_c) g} \quad \text{and} \quad \eta_t = \frac{T^2}{2(\dot{m}_a + \dot{m}_c) P_{Total}} \qquad (6) \text{ and } (7)$$

where P_{Total} includes the discharge, electromagnet, and cathode keeper power.

Another method that can be used to estimating thruster discharge efficiency is by use of a phenomenological efficiency model. The model used in this paper is same as a prior work by Shastry,[36]

$$(\eta_t)_d = \eta_v \eta_d \eta_b \eta_m \eta_q \qquad (8)$$

Where η_v is the voltage utilization efficiency, η_d is the divergence efficiency, η_b is current utilization efficiency, η_m is the mass utilization efficiency, η_q is the charge utilization efficiency. As such the phenomenological efficiency model provides insights that help in assessing the various loss mechanisms during Hall thruster operation. The voltage utilization efficiency describes, on the average, how much of the voltage provided by the discharge supply is actually used to accelerate the ions. This factor is typically measured by the RPA. The divergence efficiency describes how much of the kinetic energy imparted to the ions is axial, thrust-producing, kinetic energy. This factor is typically measured by the Faraday probe. The current utilization efficiency describes how much of the discharge current is carried by ions instead of electrons. Electrons generate negligible thrust compared to the ions. This factor is typically measured by the Faraday probe. The mass utilization efficiency describes how much of the mass flow exiting the thruster channel is in the form of ions. This factor typically requires data from the Faraday probe and the ExB probe. The charge utilization efficiency is a number of terms representing the effects of having multiply-charged species that are not already described by the other terms in the efficiency model. Detailed presentation of the far-field probe data analysis for the 300M, 300MS, and 300MS-2 is presented in a companion paper by Huang *et al*.[26] However, some of the findings from that paper will be presented during discussion of the results.

Results of the performance characterization of configurations 300MS and 300MS-2 are presented in Figs. 15 through 20 for all the test conditions. For each discharge voltage, graphs of the anode xenon mass flow rate, thrust, discharge efficiency, and discharge specific impulse as a function of discharge current are presented. The performance results for the 300M (US) are also included in the figures to facilitate discussion of the results.

Results presented in Figs. 15a, 15b, 15c, and 15d indicate that the 300MS and 300MS-2 configurations had very

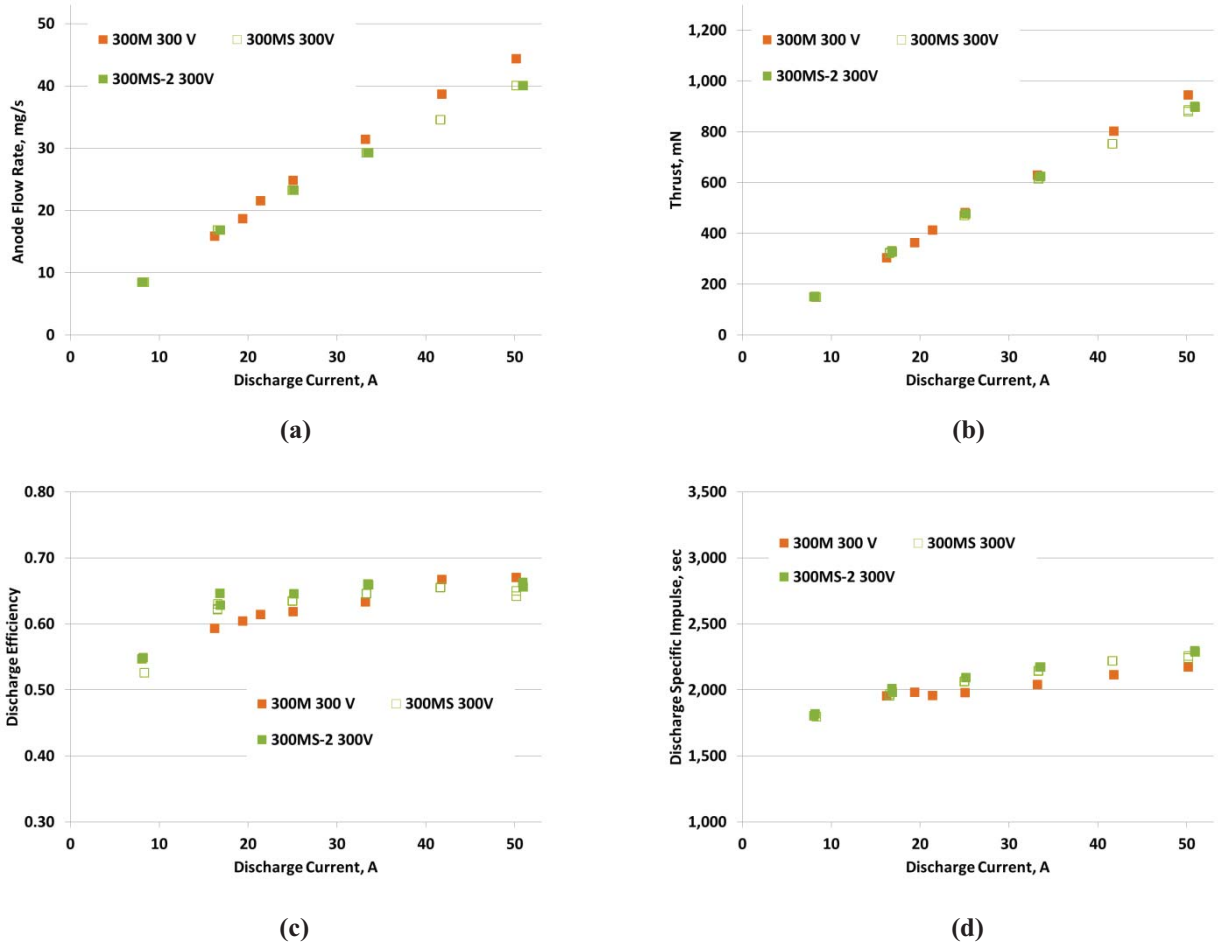

Figure 15. 300M, 300MS, and 300MS-2 anode flow rate (a), thrust (b), discharge efficiency (c), and discharge specific impulse (d) versus discharge current for thruster operation at a discharge voltage of 300 V.

similar performance at a discharge voltage of 300 V. The ratio of m_a/I_d, Fig. 15a, is almost identical considering the uncertainty in the discharge current and flow measurements. Measured thrust for the 300MS, Fig. 15b, is slightly lower than the 300MS-2 but is within the uncertainty in the thrust measurement. Computed discharge efficiency (Fig. 15c) and specific impulse magnitudes (Fig. 15d) for the 300MS are slightly lower than 300MS-2 due to the slightly higher thrust values for the 300MS-2. As such, for thruster operation at a discharge voltage of 300 V, shortening the discharge chamber did not result in degraded thruster performance. For the magnetically shielded thruster configuration, the peak discharge efficiency was approximately 65% at 12.5 and 15 kW for a discharge voltage of 300 V. A Peak discharge specific impulse of approximately 2,250 sec was attained at 15 kW. Comparing the performance of the 300MS and 300MS-2 configurations to 300M (US) indicates that the 300MS and 300MS-2 discharge efficiency and specific impulse magnitudes slightly exceed that of the 300M for thruster discharge power up to 10 kW. For discharge thruster power above 10 kW, the 300M discharge efficiency slightly exceeds that of the 300MS and 300MS-2. The higher 300M discharge efficiency above 10 kW at a discharge voltage of 300 V is attributed to the higher thrust magnitudes that resulted from higher anode flow rates. However, the discharge specific impulse magnitudes of the 300MS and 300MS-2 are consistently higher than the 300M due to the higher flow rates applied in the 300M. Analysis performed by Huang confirms these trends and shows that probe derived discharge efficiency for both the 300M and 300MS configurations at 10 and 15 kW was approximately 65%.

Results presented in Figs. 16a, 16b, 16c, and 16d indicate that the 300MS and 300MS-2 configurations had very similar performance at a discharge voltage of 400 V, as was the case at 300V. The ratio of m_a/I_d, Fig. 16a, is almost identical considering the uncertainty in discharge current and flow measurements. The 300MS measured thrust, Fig. 16b, is slightly higher than the 300MS-2 but is within the uncertainty in the thrust measurements. Computed

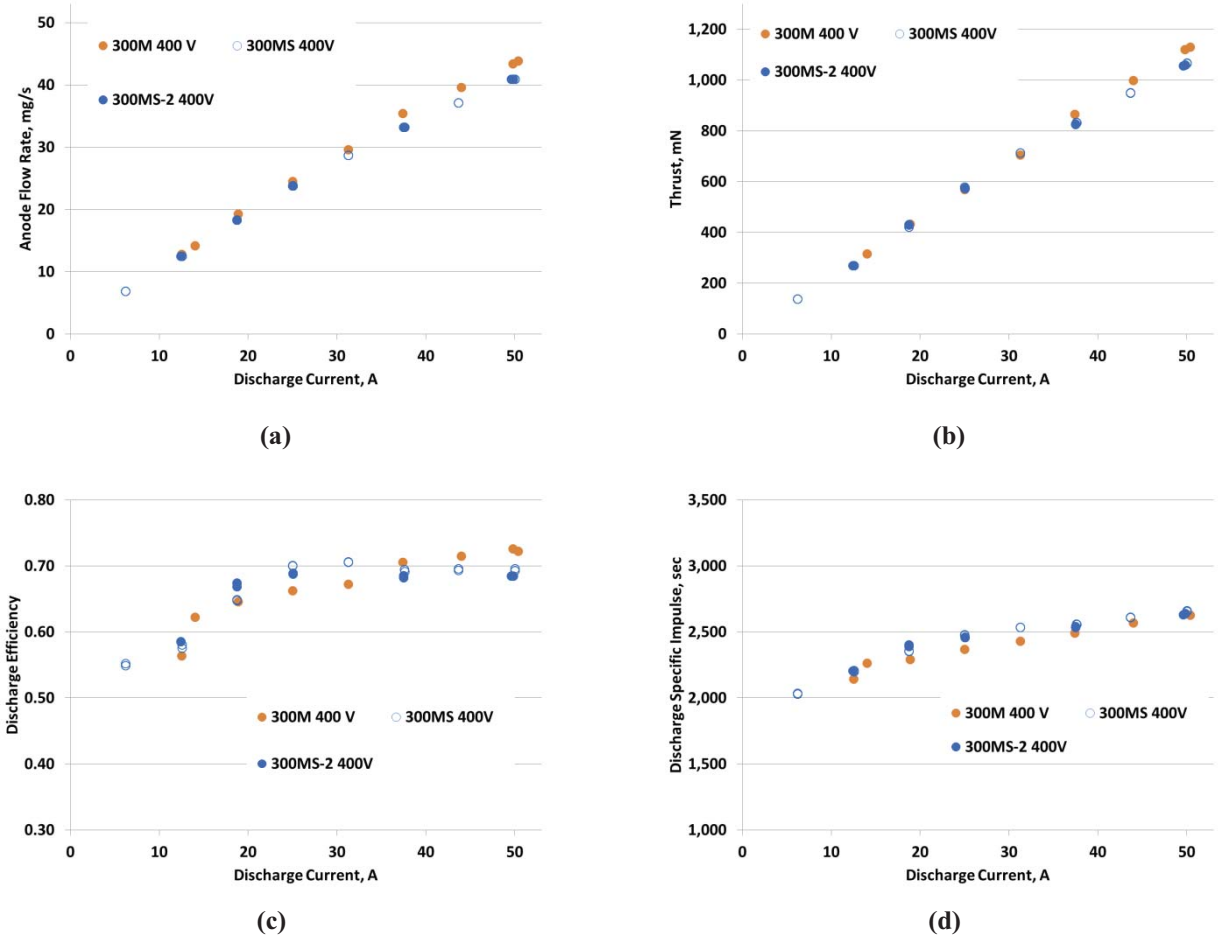

Figure 16. 300M, 300MS, and 300MS-2 anode flow rate (a), thrust (b), discharge efficiency (c), and discharge specific impulse (d) versus discharge current for thruster operation at a discharge voltage of 400 V.

discharge efficiency (Fig. 16c) ,and specific impulse, (Fig. 16d), magnitudes for the 300MS are slightly higher than the 300MS-2 due to the slightly higher thrust values for the 300MS. As such, for thruster operation at a discharge voltage of 400 V, shortening the discharge chamber did degrade thruster performance. For the magnetically shielded thruster configuration, the peak discharge efficiency was approximately 70% at power levels of 12.5 kW and above as is shown in Fig. 16c. Peak discharge specific impulse of approximately 2,650 sec was attained at 20 kW as is shown in Fig. 16d. Comparing the performance of the 300MS and 300MS-2 configurations to 300M (US) at 400 V indicates that the 300MS and 300MS-2 discharge efficiency and specific impulse exceed that of the 300M for thruster discharge power up to 12.5 kW. Results from the phenomenological model analysis at 400 V and 10 kW indicate that this improved performance is due to higher voltage and current utilization efficiencies, this is partially attributed to the improved ionization efficiency in a shielded configuration when compared to an unshielded configuration due to the higher electron temperatures.[26] For discharge thruster power above 12.5 kW, the 300M discharge efficiency exceeds that of the 300MS/MS-2. The higher 300M discharge efficiency above 12.5 kW is attributed to the higher thrust magnitudes that resulted from higher anode flow rates. However, the discharge specific impulse magnitudes of the 300M and 300MS and 300MS-2 are very similar mainly due to that fact that the higher thrust generated by the 300M is offset but the higher anode flow rates.

Results presented in Figs. 17a, 17b, 17c, and 17d indicate that the 300MS and 300MS-2 configurations had similar performance at a discharge voltage of 500 V. The ratio of m_a/I_d and thrust magnitudes are almost identical considering the uncertainty in the discharge current, flow, and thrust measurements. Computed discharge efficiency and specific impulse magnitudes for the 300MS are lower than 300MS-2 at discharge power less than or equal to 10

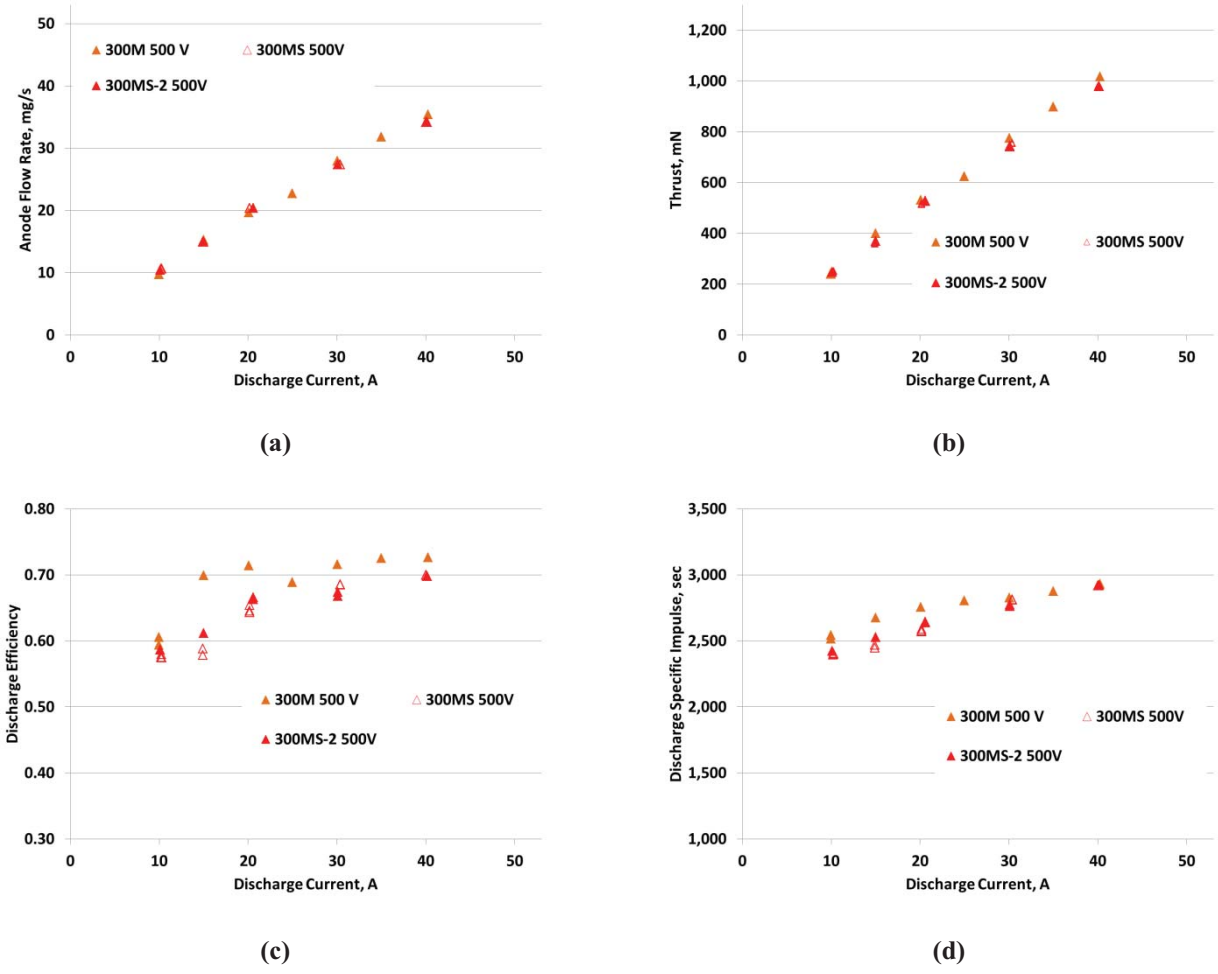

Figure 17. 300M, 300MS, and 300MS-2 anode flow rate (a), thrust (b), discharge efficiency (c), and discharge specific impulse (d) versus discharge current for thruster operation at a discharge voltage of 500 V.

kW, but become higher at discharge power levels above 10 kW, this is due to the slightly higher thrust values in the 300MS. As such, for thruster operation at a discharge voltage of 500 V, shortening the discharge chamber did not result in degraded thruster performance. For the magnetically shielded thruster configuration, the peak discharge efficiency and discharge specific impulse were was approximately 70% at and 2,900 sec at 20 kW as is shown in Figs. 17c and 17d, respectively. As for comparing the performance of the 300MS and 300MS-2 configurations to 300M, the 300M data for discharge power below 12.5 kW seems to overestimate the thruster performance. The 300M trends presented in Figs. 17c and 17d are not typical and are being reviewed. Findings from the phenomenological model indicate that at 10 kW the 300MS had a higher voltage utilization efficiency than the 300M, but the mass utilization efficiency was lower due to the higher current to mass ratio due to the higher average charge state of the shielded configuration.[26] At 20 kW the phenomenological model results indicate that the 300MS still had higher voltage utilization than the 300M but with a lower divergence efficiency, which offset the gains from the higher voltage utilization.

Results presented in Figs. 18a, 18b, 18c, and 18d indicate that the 300MS and 300MS-2 configurations had similar performance at a discharge voltage of 600 V. The trends observed at a discharge voltage of 600 V are similar to the 500 V case. For the magnetically shielded thruster configuration, the peak discharge efficiency and discharge specific impulse were approximately 71% at and 3,130 sec at 20 kW, respectively, as is shown in Figs. 18c and 18d. Comparing the performance of the 300MS and 300MS-2 configurations to 300M (US) indicates that the 300MS and 300MS-2 discharge efficiency and specific impulse are lower than the 300M for all discharge power levels except at 20 kW where they are approximately equal. Although, it might be expected that the 300M has a higher performance

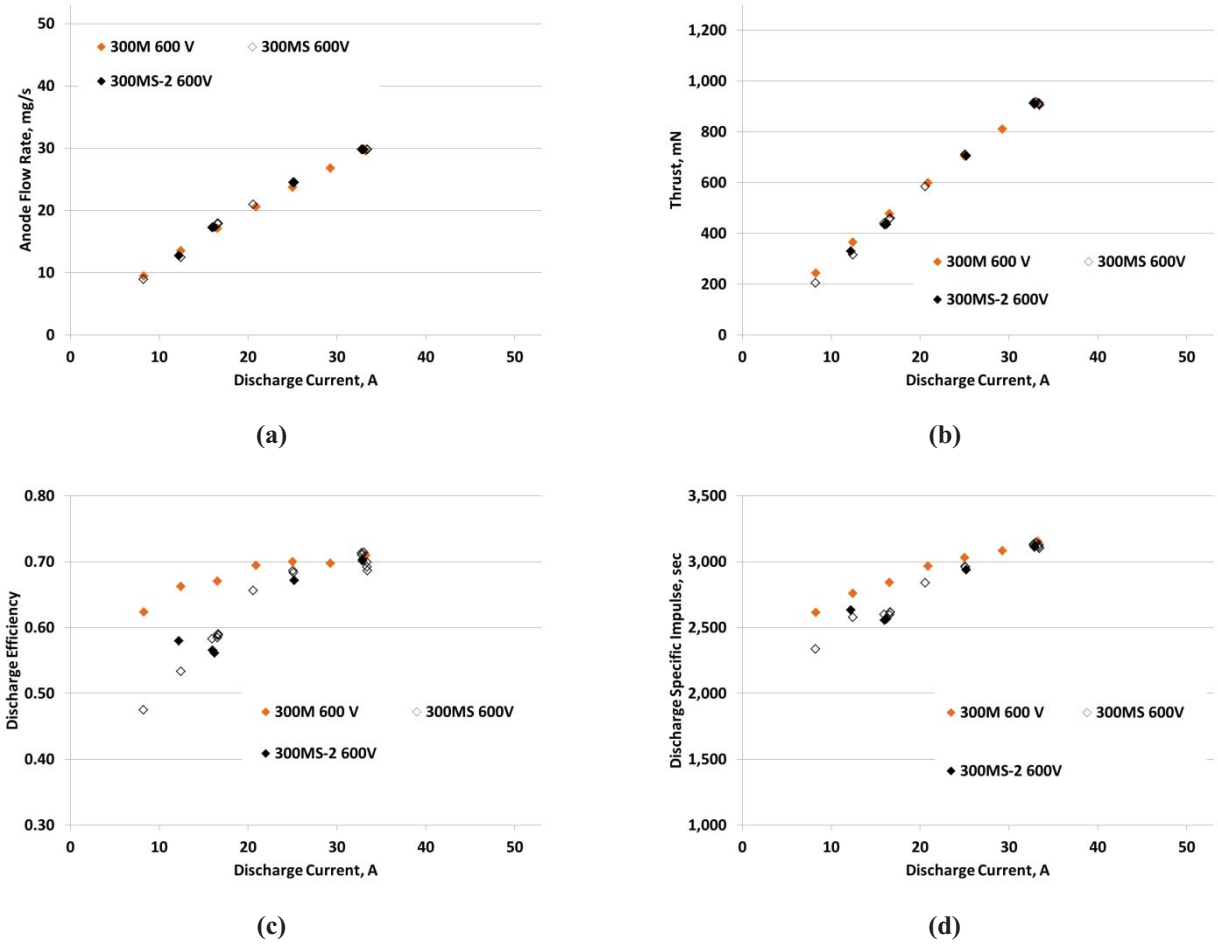

Figure 18. 300M, 300MS, and 300MS-2 anode flow rate (a), thrust (b), discharge efficiency (c), and discharge specific impulse (d) versus discharge current for thruster operation at a discharge voltage of 600 V.

at the lower flow rates (trend observed at other discharge voltage conditions), the difference between the 300M and 300MS performance seems to be higher than expected and that data will be revisited to confirm the differences. Unfortunately no far-field Faraday, RPA, E×B, and Langmuir probe data was acquired and analyzed at 600 V, but it is postulated that operation at higher discharge voltages is further reducing the mass utilization of the 300MS configuration, especially at lower flow rates, due to increased plasma charge state.

Tests were also performed at discharge voltages of 650 and 700 V for 300MS-2. Tests at these higher discharge voltages were not attempted for the 300MS because there was concern that testing at these high discharge voltages would damage the thruster and that would prohibit completion of the planned test matrix. As such, tests at 650 and 700 V were only performed for 300MS-2. Tests at these higher discharge voltages proceeded without any issues. At a discharge voltage of 650 and 700 V, the thruster demonstrated a discharge efficiency of 70% and 69%, respectively. Discharge specific impulse of 3,200 and 3,300 sec were achieved at discharge voltages of 650 and 700 V, respectively.

Figures 19 and 20 present the total thruster efficiency results for the 300M, 300MS, and 300MS-2 configurations. Results indicate that for the 300MS and 300MS-2 thruster performance increased with increasing discharge power. This is typical in Hall thruster (up to certain power and current density), since increasing discharge

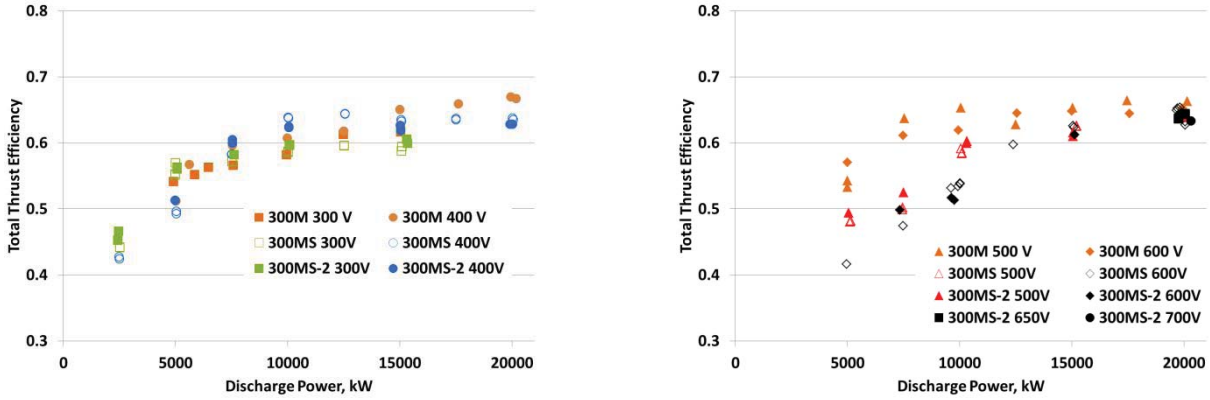

Figure 19. 300M, 300MS, and 300MS-2 total discharge efficiency as a function of discharge power.

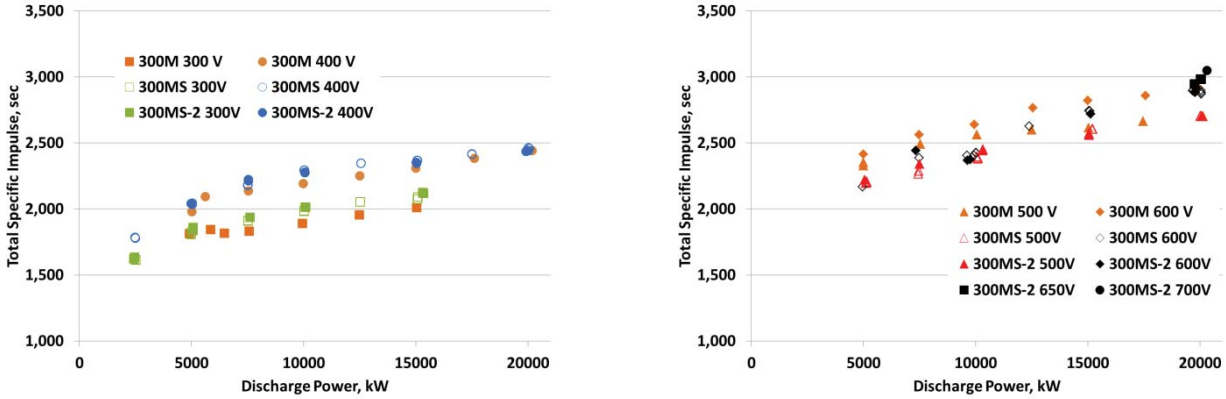

Figure 20. 300M, 300MS, and 300MS-2 total specific impulse as a function of discharge power.

power at a given discharge voltage results in higher current and plasma density which results in a higher ionization rate. Results indicate that, in general, for 300 and 400 V thruster operation the 300M performance was higher than the 300MS and the 300MS-2 for power levels above 12.5 kW, whereas for 500 and 600 V thruster operation the 300M performance was higher than the 300MS and 300MS-2 for all power levels. This may be attributed to the fact that for thruster operation at higher discharge voltages and lower power, the required magnetic field for discharge current minimization was higher than levels where magnetic circuit saturation onset would start. This resulted in the thruster operating at a non-optimal magnetic field setting with a topology that was not entirely magnetically shielded. Table 3 below lists the peak total thruster efficiency and specific impulse for the 300M, 300MS, and

300MS-2 thrusters at the different operating discharge voltages and indicates (as is shown in Figs. 19 and 20) that thruster total efficiency and specific impulse for the unshielded and shielded configurations is very similar.

Table 3. Summary of the 300M, 300S, and 300MS-2 total efficiency and specific impulse performance at peak power for the various operating discharge voltage magnitudes.

Discharge Voltage,	Discharge Power,	300M		300MS		300MS-2	
	kW	$\eta_{T,\%}$	$I_{sp,T}$, sec	$\eta_{T,\%}$	$I_{sp,T}$, sec	$\eta_{T,\%}$	$I_{sp,T}$, sec
300	15	62	2,011	60	2,088	60	2,117
400	20	66	2,441	64	2,417	63	2,442
500	20	66	2,700	64	2,702	64	2,704
600	20	65	2,912	63	2,883	64	2,881
700	20					63	3,048

In summary, the NASA Glenn and JPL effort succeeded in modifying the 300M US magnetic circuit to a shielded magnetic circuit. The total efficiency and total specific impulse of the 300MS thruster were lower than the 300M at full power. Shortening of the discharge channel of the 300MS by 20% did not adversely impact the performance of the magnetically shielded thruster. Far-field plasma probe measurements found that, in general, the magnetically shielded configuration had a higher beam divergence than the US configuration, this is attributed to the fact that the peak radial magnetic field in the shielded configuration was moved downstream from its baseline location in the 300M, this causes the ionization and acceleration zones to also move downstream. The far-field probe data, also found that the 300MS plume charge state was higher than the 300M, this is attributed to the fact that in a magnetically shielded thruster the ion flux to the chamber walls is greatly reduced which causes the electron temperatures along the discharge chamber centerline to reach higher temperatures due to the reduced cooling effects that are derived from the secondary electron emission from the ceramic discharge chamber walls. [37,38,39]

C. Thermal Characterization

Temperature measurements of selected 300MS thruster components were made. The main objectives of performing the temperature measurements were:

- Assess the thermal operating environment of the 300MS configuration and use the data to compare to similar measurements performed on the 300M; and
- Provide critical data that will be used to validate the detailed thermal models that are being developed at NASA Glenn and JPL.

To meet our objectives the following thruster components temperatures were instrumented and monitored:

- Outer Front pole at 2 o'clock position;
- Backpole at 9 o'clock position;
- Inner discharge chamber chamfered surfaces at 3 and 6 o'clock positions;
- Outer discharge chamber chamfered surfaces at 3 and 6 o'clock positions;
- Discharge chamber base at 3 and 6 o'clock positions;
- Inner electromagnet out layer at two axial locations (near and upstream of exit plane); and
- Thruster inner bore.

For the thermal characterization test of the 300MS (part of Test#3), steady state temperature data was obtained for the following operating thruster conditions:

- Discharge power of 10 kW at a discharge voltage of 400V;
- Discharge power of 15 kW at a discharge voltage of 500V; and
- Discharge power of 20 kW at discharge voltage of 400, 500, and 600 V.

Table 3 presents a summary of the 300MS steady state temperature values for the inner coil, inner boron nitride wall, and outer boron nitride wall. Table 4 also contains similar steady state temperature measurements that were made on the 300M during a previous test at very similar locations on the thruster.

Table 4. 300MS and 300M steady state temperature measurements for the inner electromagnet outer layer and boron nitride discharge channel inner and outer walls for thruster operation at 10, 15, and 20 kW. Note: shaded cells with red text color denote 300MS data.

Thruster Discharge Power, kW	Thruster Discharge Voltage, V	Inner Coil Temperature, °C				Inner Boron Nitride Temperature, °C			Outer Boron Nitride Temperature, °C		
		Downstream TC		UpStream TC		3'	6'		3'	6'	
10	300		374.8		336.6			422.7			428.1
10	400	375.6		365.1		338.9	340.9		368.4	369.7	
15	500	421.7		407.9		425.3	427.4		489.7	488.1	
20	400	438.0	529.9	421.4	467.4	457	455.9	566.4	496.3	481	573.2
20	500		535.6		478.7			546			560.3
20	600	448.0		433		456.1	457.1		541.4	531.5	

Results in Table 4 indicate that for the 300MS and 300M thruster configurations, increasing the thruster discharge power results in increased component temperatures, as would be expected. Inner and outer 300MS discharge channel temperature readings indicate that symmetric heating of the discharge channel walls was realized as indicated by the almost identical temperature readings for both the inner and outer boron nitride channels at the 3 and 6 o'clock positions. Additionally, for the 300MS configuration, the difference between the downstream (closest to discharge chamber exit plane) and upstream temperature readings of the inner coil is very small, that is an indicator that minimal preferential heating on the inner discharge channel wall due to ion impingement is taking place; this is an indication that the ions are being shielded and are not striking the downstream edge of the discharge channel as is typically the case for unshielded thrusters.

Comparing the 300MS temperature readings with the 300MS for the 20 kW 400 V case shows that: the inner discharge channel wall temperatures for the 300MS are approximately 100 °C lower than the 300M, the outer discharge channel wall temperatures are approximately 80 °C lower than the 300M, the inner coil downstream temperatures are 90 °C lower than the 300M, and the inner coil downstream temperatures are 48 °C lower than the 300M. Noting that although the inner electromagnet was operated at higher current settings during than the 300MS test than for the 300M test, its temperature was still significantly lower than during the 300M test. This is another indicator that magnetic shielding helps alleviates some of the thermal challenges that are faced when designing high power Hall thrusters.

V. Conclusions and Future Work

Numerical simulations of the 300M thruster with JPL's Hall2De physics based simulation code indicated that modifying the unshielded magnetic topology of the 300M thruster to a magnetically shielded topology will increase the throughput capability of the 300M by at least ten fold without significant reduction in thruster performance. Magnetic circuit modeling performed by MagNetV7 was used to design the new magnetic circuit components for the 300M that can be used to attain the magnetically shielded field topology specified by Hall2De.

The new magnetic circuit components were fabricated and integrated with the existing 300M thruster to create the 300MS configuration. Prior to vacuum testing, mapping of the 300MS magnetic circuit confirmed attainment of a magnetically shielded field configuration. Testing of the 300MS was performed for power levels between 2.5 and 20 kW and discharge voltages between 300 and 600 V. A 20% shorter 300MS thruster (300MS-2) was also tested up to 20 kW and 700V. Initial confirmation that magnetic shielding was attained was realized after inspection of the discharge channel surface that indicated the deposition of back sputtered materials from the facility without any signs of discharge channel sputtering due to ion bombardment. Definite confirmation that magnetic shielding was attained in the 300MS was made by use of discharge channel surface flush-mounted Langmuir probes, the probes measured anode plasma potentials and very low electron temperatures on the discharge channel chamfered surfaces near the discharge channel exit plane. Inner electromagnet, inner discharge channel, and outer discharge channel temperature measurements indicated that magnetic shielding was achieved. The temperature readings indicated that in a magnetically shielded thruster, the discharge chamber heat load due to ion impingement is significantly lower than unshielded thruster. This results in reduced thruster component temperatures and alleviates some of the thermal challenges faced during high power thruster design.

Performance evaluation of the 300MS and 300MS-2 was made. Performance test results indicated that, in general, the 300MS performance was very similar to the 300M. Peak total thrust efficiencies between 63% and 65% for discharge voltages between 300 and 700 V were demonstrated for the 300MS and 300MS-2 configurations. Total specific impulse magnitudes of 3050 sec were achieved for discharge voltage of 700 V. Far-field plasma

measurements confirmed the measured discharge efficiencies but also found that a magnetically shielded thruster may have higher plume divergence and higher charge state than an unshielded configuration. Investigation of effect of the higher plume divergence and higher charge state on thruster stability and lifetime will be evaluated.

Acknowledgments

The authors would like to thank and acknowledge the Space Technology Mission Directorate for funding this work. The authors would also like to thank Christopher Griffith for generating the drawings for the 300MS magnetic circuit components. The authors would also like to thank Kevin Blake, Kevin McCormick, and Michael Pastel for their help in machining the thruster new magnetic circuit components and thruster assembly. Lastly the authors also thank Kevin Blake, Tom Ralys, George Jacynycz, George Readus, for helping to install the thruster and motion system used in this study, as well as maintaining and operating the vacuum facility.

References

[1] Dudzinski, L., et al., "Design of Solar Electric Propulsion Transfer Vehicle for a Non-Nuclear Human Mars Exploration Architecture," 26th IEPC-99-181, October 1999.
[2] Oleson, S.R., et al., "Advanced Propulsion for Space Solar Power Satellites," AIAA-99-2872, June 1999.
[3] Oleson, S.R., et al., "Mission Advantages of Constant Power Variable Specific Impulse Electrostatic Thrusters," NASA TM-2000-210477, 2000.
[4] Jankovsky, R.S., et al., "Preliminary Evaluation of a 10 KW Hall Thruster," AIAA-99-0456, January 1999.
[5] Mason, L.S., et al., "1000 Hours Testing of a 10 KW Hall Effect Thruster," AIAA-3773, July 2001.
[6] Jankovsky, R.S., et al., "NASA's Hall Thruster Program 2002," AIAA-2002-3675, July 2002.
[7] Manzella, D. H., et al., "Laboratory Model 50 kW Hall Thruster," AIAA-2002-3676, July 2002.
[8] Jacobson, D.T., et al., "NASA's 2004 Hall Thruster Program," AIAA-2004-3600, July 2004.
[9] Peterson, P. Y., "Performance and Wear Characterization of a High Power High–Isp Hall Thruster," AIAA-2005-4243, July 2005.
[10] http://www.nasa.gov/exploration/new_space_ enterprise/home/heft_summary.html
[11] Brophy, J.R., et al., "300-kW Solar Electric Propulsion System Configuration for Human Exploration of Near Earth Asteroids," AIAA 2011-5514, August 2011.
[12] Smith, B., Nazario, M. L., and Manzella, D. H., "Advancement of a 30kW Solar Electric Propulsion System Capability for NASA Human and Robotic Exploration Mission," IAC-12-C4.4.2.
[13] Kamhawi, H., Haag, T. W., Jacobson, D. T., and Manzella, D. H., "Performance Evaluation of the NASA-300M 20 kW Hall Effect Thruster", AIAA-2011-5521,July 2011.
[14] Soulas, G. C., Haag, T. W., Herman, D. A., Huang, W., Kamhawi, H., Shastry, R. and Williams, G., "Performance Test Results of the NASA-457M v2 Hall Thruster," AIAA-2012-3940, July 2012.
[15] Herman, D. A., Shastry, R., Huang, W., Soulas, G. C. and Kamhawi, H., "Plasma Potential and Langmuir Probe Measurements in the Near-field Plume of the NASA-300M Hall Thruster," AIAA-2012-4115, July 2012.
[16] Huang, W., Shastry, R., Herman, D. A., Soulas, G. C. and Kamhawi, H., "Ion Current Density Study of the NASA-300M and NASA-457Mv2 Hall Thrusters," *Proceedings of the 48th AIAA/ASME/SAE/ASEE Joint Propulsion Conference and Exhibit*, AIAA-2012-3870, July 2012.
[17] Shastry, R., Huang, W., Herman, D. A., Soulas, G. C. and Kamhawi, H., "Plasma Potential and Langmuir Probe Measurements in the Near-field Plume of the NASA-457Mv2 Hall Thruster,", AIAA-2012-4196, July 2012.
[18] Brophy, J., and Oleson, S., "Spacecraft Conceptual Design for Returning Entire Near-Earth Asteroids,", AIAA. 2012-4067, July 2012.
[19] Hofer, R R, Jorns, B A, Polk, J E, Snyder, J S, Mikellides, I G, "Wear test of a magnetically shielded Hall thruster at 3000 seconds specific impulse," IEPC-2013-033, 33rd International Electric Propulsion Conference, Washington, DC, Oct 6-10, 2013.
[20] Mikellides, I.G., Katz, I., and Hofer, R.R., "Design of a Laboratory Hall Thruster with Magnetically Shielded Channel Walls, Phase I: Numerical Simulations," AIAA 2011-5809, July 2011.
[21] Hofer, R.R., Goebel, D.M., Mikellides, I.G., and Katz, I., "Design of a Laboratory Hall Thruster with Magnetically Shielded Channel Walls, Phase II: Experiments,"AIAA 2012-3788, July 2012.
[22] Mikellides, I.G., Katz, I., Hofer, R.R., and Goebel, D.M., "Design of a Laboratory Hall Thruster with Magnetically Shielded Channel Walls, Phase III: Comparison of Theory with Experiment,"AIAA 2012-3789, July 2012.

[23] Mikellides, I.G, and Katz, I., Numerical simulations of Hall-effect plasma accelerators on a magnetic-field-aligned mesh, *Physical Review E*, 86 (2012) 046703.
[24] http://www.infolytica.com/en/products/magnet/
[25] Shastry, R., Huang, W., Haag, T. W. and Kamhawi, H., "Langmuir Probe Measurements within the Discharge Channel of the 20-kW NASA-300M and NASA-300MS Hall Thrusters," Proceedings of the 33rd International Electric Propulsion Conference, IEPC-2013-122, Washington, D.C., October 6-10, 2013.
[26] Huang, W., Shastry, R., Soulas, G. C., and Kamhawi, H., "Farfield Plume Measurement and Analysis on the NASA-300M and NASA-300MS", 33rd International Electric Propulsion Conference, IEPC-2013-057, Washington, DC, 6-10 Oct, 2013.
[27] I. G. Mikellides, I. Katz, R. R. Hofer, D. M. Goebel, K. de Grys, and A. Mathers, "Magnetic Shielding of the Channel Walls in a Hall Plasma Accelerator," *Phys. Plasmas*, 18, 3, 033501 1-18 (2011).
[28] I.G. Mikellides, I. Katz, R.R. Hofer, D.M. Goebel, "Magnetic shielding of walls from the unmagnetized ion beam in a Hall thruster," *Appl. Phys. Lett.*, 102 (2013).
[29] Morosov, A. I., "Focusing of Cold Quasineutral Beams in Electromagnetic Fields," *Soviet Physics - Doklady* 10, 8 (1966).
[30] Morosov, A. I., Esipchuk, Y. V., Tilinin, G. N., Trofimov, A. V., Sharov, Y. A., and Shchepkin, G. Y., "Plasma Accelerator with Closed Electron Drift and Extended Acceleration Zone," *Soviet Physics Technical Physics* 17, 1, 38-45 (1972).
[31] Morozov, A.I., and Savelyev, V.V., "Fundamentals of Stationary Plasma Thruster Theory," *Reviews of Plasma Physics*, 21, 203 (2000).
[32] Katz, I., and Mikellides, I.G., "Neutral gas free molecular flow algorithm including ionization and walls for use in plasma simulations," *J Comput Phys*, 230 (2011) 1454-1464.
[33] Meezan, N.B., Hargus, W. A., and Cappelli, M.A., "Anomalous electron mobility in a coaxial Hall discharge plasma," *Physical Review E*, 63 (2001).
[34] Boniface, C., Garrigues, L., Hagelaar, G.J.M., Boeuf, J.P., Gawron, D., and Mazouffre, S., "Anomalous cross field electron transport in a Hall effect thruster," *Appl Phys Lett*, 89 (2006).
[35] Hobbs, G.D., and Wesson, J.A., "Heat Flow through a Langmuir Sheath in Presence of Electron Emission," *Plasma Physics*, 9 (1967) 85-87.
[36] Shastry, R., Hofer, R. R., Reid, B. M., and Gallimore, A. D., "Method for analyzing ExB probe spectra from Hall thruster plumes", *Review of Scientific Instruments*, Vol. 80, No. 6, doi:10.1063/1.3152218, 22 Jun., 2009, pp. 063502.
[37] Kim, V., "Main Physical Features and Processes Determining the Performance of Stationary Plasma Thrusters," Journal of Propulsion and Power, Vol. 14, No. 5, Sept.-Oct. 1998, pp. 736-746.
[38] Kim, V., et al., "Investigation of SPT Performance and Particularities of its Operation with Kr/Xe Mixtures," IEPC-01-065, Sept. 2001.
[39] Goebel, D. M., and Katz, I., Fundamentals of Electric Propulsion: Ion and Hall Thrusters, JPL Science and Technology Series, Pasadena, CA, 2008, Chap. 7.